metals

MDPI

Review

A Broad Literature Review of Density Measurements of Liquid Cast Iron

Kristina Hellström *, Attila Diószegi and Lucian Diaconu

School of Engineering, Jönköping University, 551 11 Jönköping, Sweden; attila.dioszegi@ju.se (A.D.); lucian-vasile.diaconu@ju.se (L.D.)

* Correspondence: kristina.hellstrom@ju.se; Tel.: +46-(0)36-101-527

Academic Editor: Xing-Qiu Chen

Received: 13 April 2017; Accepted: 27 April 2017; Published: 10 May 2017

Abstract: The literature on density measurements, with a particular interest in methods suitable for liquid cast iron, is reviewed. Different measurement methods based on a number of physical properties are highlighted and compared. Methods for the calculation of density are also reviewed, and the influence of alloying elements on density is, to some extent, discussed. The topic is of essence for the understanding of the material behaviour at solidification, which is pivotal in software applications for casting simulation. Since a deeper understanding of the relationship between the density of liquid cast iron and volume expansion is necessary, the conclusion that further research within the field is needed lies close at hand.

Keywords: density; experimental methods; calculation

1. Introduction

Density is defined as mass per unit volume, and its calculation formula is presented below:

$$\rho = \frac{m}{V} \tag{1}$$

Measuring the density of cast iron in its molten state has proven not as straight forward as the above formula might imply. Various methods have been employed based on the measurement of buoyancy, hydrostatic pressure, volume, or shape [1]. Some of the more frequent methods will be reviewed below. They all have their advantages and disadvantages, and, while some of them are used mainly for measurements of other properties, they are commonly used for density measurements as well. One of the things most methods have in common is that the density must be calculated by one or several operations from data obtained in a direct or indirect way.

As one of the thermophysical properties, density plays an important part in the solidification of castings. With the increasing use of simulation software to predict casting outcomes, it has become even more important to base the calculations on reliable data to obtain consistent results. Different theoretical methods for calculations of density will therefore also be reviewed.

A general overview of the density-temperature functions and the chemical compositions of the materials used in the reviewed literature can be found in Figure 1.

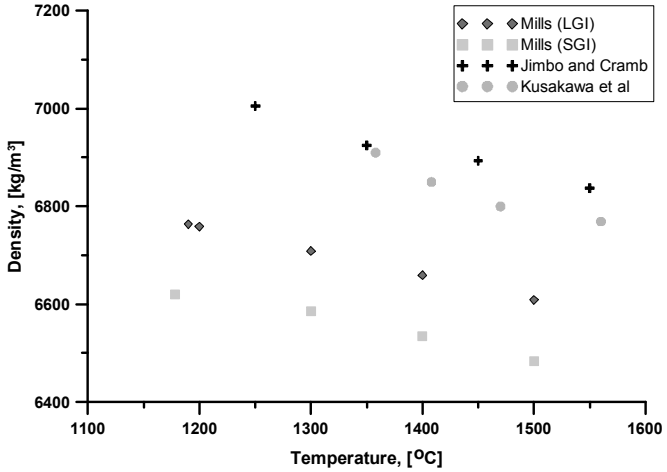

Figure 1. Density of molten cast iron from the literature data. (Mills [2] for lamellar and spheroidal graphite iron, Jimbo and Cramb [3] for lamellar iron, and Kusakawa [4] for lamellar iron). Chemical composition can be found in Table 1.

Table 1. Chemical composition of the alloys in Figure 1. (Mills [2] for lamellar (LGI) and spheroidal (SGI) graphite iron, Jimbo and Cramb [3] for lamellar iron, and Kusakawa [4] for lamellar iron).

Authors	C	Si	Mn
Mills (SGI)	3.61	2.91	0.65
Mills (LGI)	3.72	1.89	0.66
Jimbo and Cramb	3.91	-	-
Kusakawa et al.	3.7–3.8	2.6–2.7	-

Scientists have been trying to measure the density of metals for a very long time. However, the existence of various measurement methods indicate that the task is not an easy one. The data on density values that can be found in the literature are predominantly on pure metals. The works that focus on cast iron are limited and are also quite widespread over time. If we consider that cast iron is not just one material, the data for each variety become even more limited.

2. Literature Review

2.1. Why Measure Density

In order to obtain accurate results from numerical simulations of, for instance, casting processes, knowledge of the thermophysical properties of the chosen alloy is pivotal. How accurate these data are determines the accuracy of the whole simulation [3,5]. A thorough knowledge of the density variations will enable simulation of heat conduction, solidification, elastic-plastic deformation, and fluid flow, which in turn will improve product quality [6].

The materials used in technical applications are often multicomponent alloys. The development of these materials is often performed empirically by mixing components until the desired properties have been achieved. However, a more time and cost efficient way would be through the use of numerical modelling. A limiting factor thus far has been the accuracy of the data available on thermophysical properties. Since density is one of the more fundamental thermophysical properties, it is of great importance to have access to the precise values. As it is also a parameter at the measurements of, for example, surface tension, viscosity, and thermal conductivity, the inaccuracy will affect these parameters as well [7].

The need for knowledge in the area of thermophysical properties is two-fold; on the one side, in the solution of problems arising in industry and, on the other, as input data for mathematical

modelling. In the latter application, it has proven a valuable means in the enhancement of process control and product quality [8].

One of the more detrimental defects in cast iron is shrinkage cavity or shrinkage porosity. The formation of these are closely linked to the volume changes taking place during solidification [4]. It is generally known that spheroidal graphite iron (SGI) and compacted graphite iron (CGI) are more prone to this kind of defect than lamellar graphite iron (LGI) is. From experiments, it has been seen that the expansion of SG iron was smaller than that of LGI and that the behaviour of compacted graphite iron was intermediary to that of lamellar and spheroidal graphite irons. Though SGI may have a lower expansion rate than LGI with the same chemical composition, the temperature range at which eutectic solidification takes place is wider for SGI. It would also seem that for SG irons the cooling rate, rather than the composition, influences the amount of expansion [9].

The propensity for micro shrinkage in cast iron is believed to be related to the amount of graphite expansion during solidification [10]. Thus, controlling the graphite expansion will be a tool for controlling micro porosity. To be able to control micro-shrinkage will also improve the mechanical properties [11].

The structure of the material, i.e., metal and alloys, has an influence on the value of the thermophysical properties [8]. In the case of density, however, that influence is regarded to be small. (For slags and glasses, on the contrary, the structural effects are much larger.)

2.2. Cast Iron

The term cast iron is used to refer to an alloy of iron and carbon, with a carbon content above 2 wt. %. The concept, however, hosts a whole family of materials. To start with, there are the differences in graphite shape—lamellar, compacted, and nodular—which will result in differences in thermal conductivity [12] and mechanical properties [13]. Moreover, the additions of various alloying elements will promote different types of matrices, which will influence the material properties to a large extent [14]. Further, while some authors advocate that the solidification of cast iron, regardless of graphite shape or carbon equivalent, will start in the same manner, i.e., by the growth of dendrites, others claim that hypereutectic irons will start to solidify by the precipitation of primary graphite. Differences in the solidification mode between lamellar, compacted, and spheroidal graphite iron have nevertheless been reported. For instance, the solidification mechanism for compacted graphite iron has been regarded as different from that of the nodular and lamellar graphite irons [10]. It has also been argued that CGI solidifies with a larger recalescence than both LGI and SGI [15] and that its displacement behaviour has been seen to be different from the LG and SG irons [10]. It has also been indicated that magnesium treated castings have longer solidification times than untreated cast iron under the same conditions. The conclusion that graphite morphology influences the solidification rate has therefore been drawn [16].

2.3. Solidification

The solidification of cast iron, as well as most materials, will start as a result of the differences in heat (energy contents) between the melt and the surroundings, i.e., the mould and the ambient air. When the energy is decreasing, the constituents of the melt will have to find a way to order themselves in a manner that is the most advantageous from an energy point of view. The atoms which have previously been disarranged are now forming an ordered crystal structure [17].

The energy transport that occurs during solidification is well described in the literature on thermodynamics. The equations that describe this mechanism consists of relations between thermophysical properties, of which density is one of the more fundamental. It is also these equations that constitute the foundation for much simulation software.

The solidification of hypoeutectic grey irons generally starts with the nucleation and growth of austenite dendrites, thereby causing a more rapid increase in density than does the cooling melt. This increase is soon followed by a decrease when the lower density graphite precipitates [10].

In hypereutectic grey iron, the increase of melt density with temperature has been seen to slow down when the temperature reaches below the liquidus temperature, indicating the precipitation of primary graphite [4].

Investigations of the solidification of cast iron employing the DAAS (Direct Austempering After Solidification) treatment could reveal austenite grains in samples cooled to room temperature. The grain size turned out to be rather large, and each grain contained several eutectic cells. Conclusions were made that austenite dendrites provide a large number of seeds for the eutectic austenite to grow on and that both hypo-and hypereutectic grey iron start to solidify by growing austenite dendrites [18]. In a later work [19], the idea was further developed that cast irons of widespread CE (carbon equivalent) values and of all graphite morphologies solidify in a similar way, i.e., that 'solidification begins with the nucleation and growth of austenite dendrites' [19] (p. 49). A dissimilarity, however, was that the CGI specimen in the study showed a much finer grain structure than the lamellar and nodular irons. Since the austenite of the eutectic cells share the same crystal orientation as the dendrite network making up the grain, it is hard to believe that the eutectic cells have been formed independently in the melt and then adhered to the dendritic network.

2.4. Instruments/Methods

As previously mentioned, many different methods have been employed to measure the density of pure metals and alloys. The techniques are based on, for example, buoyancy, hydrostatic pressure, volume, or shape. There are also techniques that use radiation or electric current in order to measure density.

2.4.1. Archimedean Method (Buoyancy)

Perhaps the oldest and most well-known method of measuring density is through the use of the Archimedean principle, which says that 'when a body is completely or partially immersed in a fluid, the fluid exerts an upward force on the body equal to the weight of the fluid displaced by the body' [20] (p. 432). The method is thus based on the measurements of the buoyancy force [1] that can be made either on the immersed body, wherein the density of the liquid has to be known, or on the liquid with a body of known density. In the case of liquid metals, a setup with a sinker and a counter weight suspended from an analytical balance has been used [21]. The sinker was immersed in the fluid and the weight loss was measured together with corresponding measurements of the temperature of the fluid. The Archimedean method has also been employed in [22]. In order to obtain reliable results from this kind of measurement, a number of corrections must be made [21]. In the case of measurements of a liquid, the expansion of the sinker must be known and taken into account, as well as the thread suspending the sinker. Also the surface tension must be known, as well as the contact angle [23]. An advantage is that the method can be used continuously as the temperature changes [24].

2.4.2. Pycnometric Method (Volume)

The pycnometric method involves a vessel of known volume and the weighing of the solidified sample. The vessel is completely filled with liquid metal and then left to solidify. From the known volume of the vessel and the weight of the sample, the density can be calculated at the temperature when the vessel was filled. The method has been used for investigations of lamellar and nodular iron [4] by employing a silica crucible with a lid on top. The method is considered accurate if the volume of the vessel is truly known [25]. The vessel material should not react with the liquid poured into it and it should have a known and preferably low coefficient of thermal expansion. The method cannot be used for continuous monitoring of the expansion and contraction behaviour of the metal with temperature; instead it gives a value of the volume at the temperature when the melt was poured to completely fill the vessel.

2.4.3. Maximum Bubble Pressure Method (Hydrostatic Pressure)

The maximum bubble pressure method allows measurements at high temperatures; however, not continuously but rather at one temperature at a time. It is based on the measurement of the pressure required to form a bubble of an inert gas at the end of a capillary immersed in the liquid metal [24]. The method employs measurements at two different levels or depths in the liquid, and from the difference in pressure required to form a bubble at these two levels, the density can be calculated [25].

The method is not regarded as accurate as the pycnometric method [25] but has the advantage over the Archimedean method in that the surface tension of the liquid does not have to be known, provided the contact angle does not change [24]. Another advantage is that the thermal expansion of the crucible does not need to be considered. However, the temperature has to be kept stable during all the two-level measurements.

Measurements can be performed either with one or with two capillaries. In the case of one capillary, a reposition procedure must be performed (i.e., the capillary should be immersed further into the melt), in which case corrections must be made to account for the change in liquid surface level [24].

The method generally requires high precision in the positioning of the capillary tip. The thermal expansion of the capillary tip must also be taken into account [24]. It may also be that bubbles leave the capillary before they are 'mature'. The data on the variation in pressure will thus be scattered. Adjustments to the capillary tip, making the walls curve, have therefore been made in some experiments [26].

An experimental setup in which measurements have been made in an atmosphere of argon, thereby reducing the levels of oxygen around the sample, has also been reported. As a clean surface was created before each bubble, the method was judged to be less sensible to oxidation and evaporation compared to the sessile drop method and electromagnetic levitation [27].

2.4.4. Sessile Drop (Shape)

The sessile drop method employs a cylindrical sample of known mass and volume, which is melted to form a drop on a flat surface or substrate (Figure 2). It is important that the drop forms symmetrically, which is most likely if the initial sample is a cylinder with sharp edges [25]. However, cylindrical samples that were conical at the top and chamfered at the bottom have also been used [6].

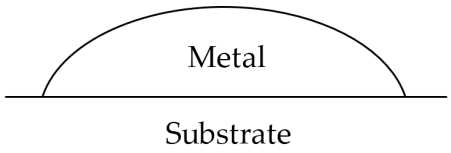

Figure 2. Schematic picture of a sessile drop.

The shape of the drop, obtained by X-ray pictures or CCD (charge coupled device) camera, is then used to calculate the volume of the drop. The method allows continuous monitoring of the drop at different temperatures. The shape of the drop is often measured from different angles, e.g., by rotating the sample [6]. The sample temperature can be detected by a thermocouple in the chamber. With the knowledge of the mass of the drop, together with the volume of it, the density can be obtained [3,6].

Measurements employing this technique are often performed in an atmosphere of argon gas or a mixture of argon and carbon monoxide. Calculations of the volume of the samples assume drop symmetry and are often done by an image sectioning technique and a curve fitting method [3,6].

The method is regarded as accurate if the drop is fully symmetrical [25]. However, the accuracy of the calculated density when the drop is not fully symmetrical can be improved by employing different algorithms for the best curve fitting.

2.4.5. Levitation Technique (Shape)

Density measurements employing the levitation technique are, just as the sessile drop method, aimed at measurements of sample volume, which, together with the weight of the sample, will give the density. The method is containerless and can therefore be used for metals that are highly reactive [1] or (deeply) undercooled [28]. The levitation of a liquid sample in the form of a sphere can be made in three ways; aerodynamically, electrostatically, or by electromagnetic forces [25]. In the case of aerodynamic levitation, the sample is supported by a gas, e.g., argon or argon-hydrogen (Figure 3). It has been regarded as a simple, robust, and versatile method [29]. The samples are, in this case, melted by laser radiation and the temperature is measured by one or several pyrometers. The shape of the drop is recorded by one or several high-speed cameras positioned at different angles. Calibration is done by using one or several spheres of known diameter, which will enable the conversion of pixels to mms. The density, ρ, of the drops can be calculated by:

$$\rho = \frac{3m\sqrt{4\pi}}{S^{3/2}}, \tag{2}$$

where m is the mass of the drop (measured directly after the experiment) and S is the surface area of the drop projection on a plane.

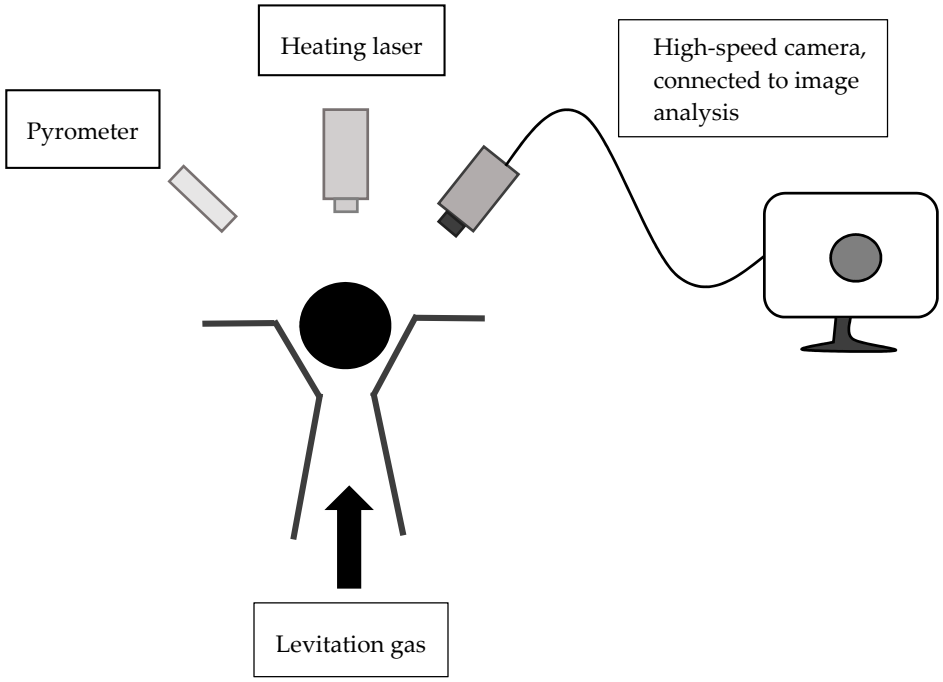

Figure 3. Schematic picture of aerodynamic levitation. Inspired by Wille et al. [29].

Electromagnetic levitation is often used for metals with high conductivity [28]. By running electrical current through a coil, an electromagnetic field is created. This will induce currents in the sample, resulting in a Lorenz force, which will position the sample through balancing the gravitation force. The samples will heat up and melt because of material resistivity [30]. A vacuum chamber surrounds the process, and measurements are performed in an atmosphere of argon or helium. The process gas is also used to cool the sample and thereby achieve temperature control. Temperature is measured by pyrometer, and drop shape is recorded by CCD cameras [7,28]. The edge of the drop is usually detected by an algorithm, and, due to oscillating effects, as many as 1000 frames are caught in order to obtain an average value [7]. This average value of the drop shape is then fitted to Legendre polynomials [28]. Since the electromagnetic field and gravity influence the shape of the drop,

full sphericity will not be achieved. However, symmetry is found around the vertical axis and the volume of the drop can be calculated by a rotational integral from the coefficients obtained by curve fitting [7,28].

In the case of electrostatic levitation, electrodes are controlling the *x*-, *y*-, and *z*-positions of the sample. Initially the sample is placed on the bottom electrode, which is grounded positively. The top electrode is then charged with high negative voltage, which makes the positively charged sample reach its levitated position, predefined by two laser beams. The voltage is then adjusted to keep the sample floating. Heating and melting are made by CO_2 heating lasers. Due to out-gassing during this process, the sample may lose its charge and fall. This can be helped by using UV-light to charge the sample. Edge detection and volume are achieved in the same way as in the electromagnetic levitation method [31].

The advantage of the levitation methods is that they are containerless and thereby apt for investigations of highly reactive metals or undercooled liquids [25,28]. The disadvantages are that symmetry is required and that oscillations of the surface have to be evened out [32]. The method is regarded as inferior to the pycnometric and Archimedean methods [25].

2.4.6. Gamma Radiation and X-ray Attenuation Techniques

The gamma radiation attenuation technique employs a γ-ray, which is passed through the liquid metal. A radiation counter records the attenuated beam [25]. The X-ray attenuation technique works in a similar manner and was first developed for the study of density changes in liquid metals that have a low liquidus temperature. The basis of the measurements is that changes in gamma or X-ray attenuation accompany changes in the density of the metal. The intensity of the beam of radiation transmitted depends on the density, thickness, and an absorption coefficient of the sample [33].

The sample is placed in a crucible in a furnace, where inert gas, e.g., helium, flows through the measurement chamber. The X-rays, which are detected on the other side of the sample, have been attenuated not only by the sample itself but also by the crucible, the gas, and some other components present at the measurement. Should the influence of these factors on the measured density values be large, corrections must be made [33].

The advantage of the method is that the surface tension of the liquid metal is not involved, neither is any chemical contamination of the liquid surface [25].

The method has also been used by researchers in the geophysical field, often to investigate the density of liquid metals, e.g., iron alloys, under high pressure [34,35]. It is then also possible to test samples of metal powders.

2.4.7. Fast Pulse Heating

The fast-pulse-heating method is no doubt very fast, with heating rates up to 108 K/s and a typical experimental time of 50 μs [36,37]. The sample, a thin wire (e.g., 0.5 mm in diameter and 50–70 mm in length), is heated from room temperature up until the end of the liquid phase, where it will 'explode', once it has reached the boiling point. Heating is made by passing a large current pulse through the sample, which thus must be made of an electrically conducting material and display ohmic resistivity [37]. Since the method is very fast, it is possible to create a liquid column, thereby avoiding the negative aspects of a vessel containing the sample. The experiment can be performed in an atmosphere of nitrogen [38], but, as the experimental time is short, chemical reactions will not affect the measurements [36]. Calibration is made by relating the known liquidus temperature to the temperature measurements of the high-speed pyrometer. (Melting will display a plateau in the voltage output of the pyrometer [37].) The volume changes of the wire-shaped sample are registered by a CCD camera every 5 μs. The pictures that are taken will display how the sample radius or diameter behaves. However, the camera is only focused on a small and limited portion of the sample [36]. Density is then calculated from the data on temperature dependent current, voltage, and sample geometry [37].

2.4.8. Dilatometer (Volume)

Dilatometers are used to measure volume changes caused by a physical process; in the case of metals and alloys, this process will most often be heating. There are different types of dilatometers; capacitve, optical, laser, and push rod are perhaps the most well-known varieties. Measurements can be performed in the horizontal or vertical direction.

The method is based on the principle that a material will change its volume if heated and that this change should be possible to read from a scale or equal. The modern dilatometers are connected to data loggers and software of some sort. Calculation of the density can be done with the knowledge of the bulk density at room temperature and the volumetric expansion of the material, measured continuously with temperature by the dilatometer [5].

The push-rod dilatometer can be equipped with one [39] or several pushrods. Several pushrods would be used for differential measurement [40]. In either case, the push rods are connected to a measurement device, often a LVDT (linear variable differential transformer) [40], monitoring the movements of the push-rod. Measurements are often made in an inert atmosphere, frequently argon or helium. Samples that will be subjected to melting are encased in a container, e.g., a hollow cylinder with a piston on each side, which will follow the expansion and contraction behaviour of the sample. The temperature is measured by one or several thermocouples, either adjacent to the sample [39], spot welded to the sample [40], or inserted in the container wall [41].

Measurements by laser dilatometer are performed either by monitoring the volume change of the whole sample directly [42] or by monitoring the movements of a device attached to the sample. An example of the latter is the investigation of lamellar and nodular graphite irons in [9]. Cylindrical samples were put in an alumina crucible and placed in the dilatometer equipment. Melting was done in an argon gas atmosphere. A pyrophyllite float on the surface of the melt was connected to a quartz rod and the displacement of the melt surface was monitored, via the movement of the rod, by an infrared-ray sensor. The temperature was measured by thermocouples.

The advantage of laser dilatometry over push-rod is that the volume changes can be monitored without the contact of a rod or likewise [43].

Literature on the use of *optical dilatometry* for measurements of cast-iron density is sparse. However, the method has been used on magnetite pellets [44] where a light source, a tube furnace and a microscope with image capturing and recording facility had been aligned horizontally. In contrast to the push-rod dilatometer, the area changes of the samples were measured. The measurements are in the case of optical dilatometry contactless, contrary to the push-rod method.

Capacitive dilatometers are used for very small samples [45] of materials used in electronics.

An example of a liquid-to-solid dilatometer can be found in [10], in which cylindrical castings in a mould of sand enclosed by steel plates were used. A quartz rod in a quartz tube was inserted in one of the cylinders, near its periphery, and connected to a LVDT in order to monitor the movements of the poured sample. The temperature was measured by a thermocouple inserted in the same cylinder at the opposite side of the quartz rod. Another example can be found in [11], in which measurements were carried out in both x- and y-direction simultaneously.

2.4.9. Draining Crucible Method

The draining crucible method has been developed and used for light metals, i.e., aluminium and magnesium [46,47]. It has the advantage that it is possible to obtain values on surface tension, viscosity, and density from the same measurement. However, the temperature during the experiment is kept constant. The method encompasses a crucible with a hole at the bottom through which the melt can run. At the beginning of the experiment, the passage is blocked. The melting is done by induction heating, and, once equilibrium conditions of the melt have been reached, a stopper rod is released and the melt will flow through the orifice down on a pan, under which a load cell is placed. Data is collected from the thermocouple and the load cell. The mass flux can then be calculated and, through

further hydrodynamic analysis of the data, the density can be determined [8]. (The method is regarded as ideal for measurements of slags and glasses.)

The diameter of the orifice must be known accurately in order not to result in significant errors in the property values [46,47]. It is also important that the material at the orifice is non-wetting with regard to the evaluated melt. The experiment can be performed in a chamber with an inert atmosphere. For temperature measurement, a thermocouple immersed in the melt has been used.

In all measurements encompassing containment of the sample, it is important to select a container material that does not react with the sample. To avoid any such reaction, containerless methods have been developed [8].

2.4.10. Other Techniques

Density can also be determined by the use of X-ray diffraction. However, because of the lack of long-range order in the liquid state, it has been seen as a complicated method for molten alloys. Still, an example of a method developed for the purpose can be found in [48].

2.5. The Effect of Alloying Elements on Density

As previously mentioned the label 'cast iron' refers, in reality, to many materials, tailored by chemical composition and cooling rate to display suitable properties for the application at hand. Additions of different elements can affect the material to show either higher tensile properties, high wear resistance, or high thermal conductivity, to mention a few implementations. However, the addition of these other elements will affect both the lattice structure and the density of the material [49].

Cast iron is often regarded as a ternary alloy of iron, carbon, and silicon. There are also some amounts of manganese, phosphorus, and sulphur in what is called unalloyed cast iron [50]. Alloying elements are elements present to an extent greater than 0.10% (except for boron and nitrogen, which are regarded as alloying elements in amounts of 0.001%) [51].

It is well known that some elements have a high graphitization effect; the addition of, for instance, carbon, boron, silicon, phosphorus, or sulphur will promote graphite formation. The mechanism at work is the effect a certain element will have on the solubility of carbon in the melt. Elements like titanium, vanadium chromium, and manganese, on the other hand, have a high positive solubility factor, meaning carbon will amalgamate with the melt, and are therefore more likely to promote the formation of cementite [52].

At the solid-state transformation, some elements are promoting pearlite (e.g., Cr, Cu, Mn, and V); others ferrite (e.g., Si, Al, and Mo). The fraction of the phases in a cast iron material affects the density, since they have different densities [53].

Since certain elements are prone to be incorporated in the solidifying phase and others less disposed, there will be an uneven distribution of elements throughout the solidified material, i.e., segregation effects. The density at a certain position will most likely be different from that in another position, with a different local chemical composition. It has been shown that there is a propensity for shrinkage porosity to form at grain boundaries [54], which are often the areas last to freeze. The chemical composition in these areas is different from the rest of the material and so is the density, most likely.

Metal atoms are arranged in an ordered crystal structure. It could be described as a unit that repeats itself over and over again in all three dimensions, making up a lattice. The unit could be organised in different ways. For iron, the fcc (face centered cubic) and bcc (body centered cubic) structures are the important ones [55]. Carbon, on the other hand, is arranged in a hexagonal structure [56].

It has been observed that there is a difference in thermal expansion behaviour whether the material is ionically bonded, metallic crystal, or covalently bonded crystals. The linear thermal expansion coefficient, α, is a scalar in cubic crystals independent of direction. In noncubic materials, on the other hand, the crystallographic direction is important for the value of α [57].

2.5.1. Carbon

In cast iron (LGI, CGI, and SGI) carbon is to a large extent present as graphite. There is, however, some carbon in the other phases as well, perhaps predominantly in austenite (2.05% at 1145 °C) and pearlite (0.8%) but also, to a minor extent, in ferrite (0.035% at 723 °C). Cementite (Fe_3C), which is one of the constituents of pearlite, has a carbon content of 6.7% [55].

The melting point for carbon is 3370 °C, and the density at 20 °C is 2.2 g/cm^3 [58]. Precipitation of graphite occurs during the eutectic solidification of lamellar, compacted, and spheroidal graphite irons. Since it has a lower density than the iron-based austenite, it will lead to an overall increase in volume and a decrease in density of the material. If the amount of expansion is related to graphite shape, it has been seen that the expansion in CGI is smaller than in LGI and SGI [10].

Graphite has a hexagonal structure [55] but is also present as an interstitial in the iron lattice. The austenite phase being an fcc-lattice gives an octahedral space between the iron atoms, a space where interstitials will fit [59]. If the interstitial atom is larger than the space, it will expand the lattice (Figure 4). Carbon exceeds this interstitial space (as does nitrogen). A simple model for volume change caused by an interstitial is provided by the following equation (Equation (3)):

$$\frac{\Delta V}{V_0} = \left(1 + \frac{\Delta a}{a}\right)^3 - 1 \tag{3}$$

where V_0 is the initial volume, ΔV is the change in volume, a is the lattice parameter, and Δa is defined as:

$$\Delta a = \frac{r_h + r_i - \sqrt{2} r_h}{\sqrt{2} r_h} \tag{4}$$

where r_h is the radius of the host atom and r_i the radius of the interstitial.

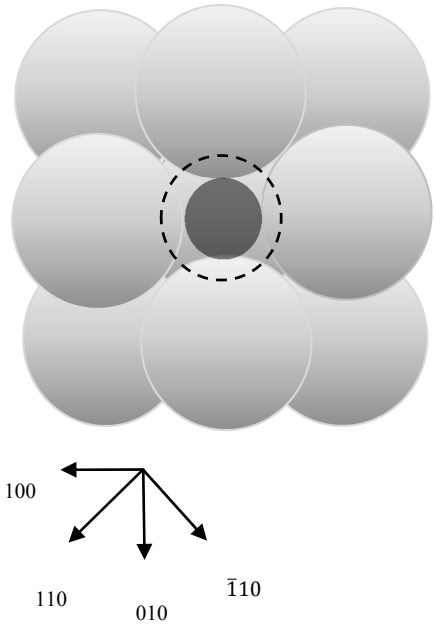

Figure 4. The fcc unit cell. The full light circles denote face centred atoms, and the shaded circle in the centre embodies maximum diameter where an interstitial atom could fit. The dashed circle shows the size of a carbon atom relative the iron atoms. Axes of the cubic cell are along the <100> directions; close packing appears along the <110> directions. Original figure from Ledbetter and Austin [59], Materials Science and Technology, www.tandfonline.com. Reproduced with permission from [59], Taylor & Francis Ltd., 2017.

However, even if the austenite lattice parameter is increased by carbon in solution, it has been claimed that the effect on the expansion coefficient is small [60]. In a liquid state, it has been argued that there is a solubility limit for a carbon atom in the interstitial position before it will start to expand the iron lattice [26].

2.5.2. Silicon

After carbon, silicon is the most common alloying element in cast iron and is sometimes seen as a ternary alloy consisting of iron, carbon, and silicon. It is a non-metallic element, however, with a metallic-like surface [61]. The melting point is 1410 °C, and the density at 20 °C is 2.33 g/cm^3 [58]. Pure silicon has an octahedral crystalline structure (just like diamond). It reacts with metals to form silicides [62], and it also binds oxygen to form SiO_2 and SiO [63].

The density for silicon at the melting point is 2.30 g/cm^3 in the solid phase and 2.51 g/cm^3 in the liquid phase. The volume increase at the transition from liquid to solid is 9.1% [63].

In the cast-iron industry, silicon is often added in the form of ferrosilicon, an alloy consisting of various degrees of silicon and iron. The density varies with the chemical composition of the compound (and the temperature) [63].

In cast iron, silicon segregates inversely, which means that it is incorporated in the solidifying phase, while the melt is deprived of its contents [64].

The amount of silicon present has been seen to influence expansion during the solidification of cast irons. The expansion of spheroidal graphite iron was smaller than that of flake graphite iron, and the behaviour of compacted graphite iron was intermediary to that of the flake and spheroidal graphite irons. For SG irons, the cooling rate rather than the composition influenced the amount of expansion [9].

Silicon has a strong graphitising effect. It has also been seen that the graphite particle density in CGI is increased with increasing additions of silicon. However, this effect may be due to the foundry grade FeSi, since inoculation in itself has been seen to increase nodularity [14].

It is generally considered that silicon acts as a deoxidiser, and it is therefore used to bind oxygen in steel melts. Other deoxidisers (Al, Ca, and Mn) are added together with Si to increase the effect. Cast iron generally contains 2–3% Si [63]; adding silicon influences the formation of the different phases, wherein ferrite is promoted and the pearlite is coarsened [52]. Silicon results in the promotion of a ferritic matrix if added in larger amounts than normal [51]. The decrease in pearlite content is due to the effect on the transformation temperatures; silicon broadens the range between stable and metastable temperatures [14].

Ferrosilicon is also used as carrier for barium, strontium, calcium, and titanium, which are added to improve the precipitation of graphite [63].

Silicon lowers the solubility of carbon in austenite [52] according to the formula:

$$\%\,\mathrm{C} + \frac{1}{16} \times \%\,\mathrm{Si} = 2.0 \tag{5}$$

Austenite can be considered a solid solution of iron and silicon in a substitutional matrix with carbon as the interstitial. Silicon has an influence on the lattice spacing in austenite, making it contract. It also has an influence on the solubility of carbon in austenite and thereby an indirect influence on the specific volume, i.e., the inverted value of the density [65].

Silicon is frequently used in electronics, wherein the material is a single crystal with the [111] or the [100] orientation. It has been shown that the thermal expansion of this type of crystal depends on the crystallographic orientation [66]. It has also been found that silicon (doped with either Sb, B, or Ga) has a constant thermal expansion coefficient at and below melting temperature (1410 °C) [28].

The effects of carbon and silicon on the density of spheroidal and flake graphite irons have also been investigated. A change in the rate of density change with temperature, $(\mathrm{d}\rho/\mathrm{d}T)$, at the liquidus temperature, something that was concluded to be caused by graphite crystallisation (CE approx.

4.6–4.7), was found. It could also be clearly seen that silicon had a greater effect on the density than carbon did [4].

2.5.3. Other Elements

When it comes to other alloying elements, they may also have an influence. For instance, in the case of molybdenum, it has been found that Mo atoms are approx. 30% larger than iron atoms [67]. They also increase the volume of the unit cell by 45%. The authors discuss the fact that molybdenum prefers a bcc structure, and, in this case, it has been placed in an fcc one.

Due to the higher solubility of copper in austenite than in ferrite, the precipitation of an ε-phase can occur, inhibiting grain growth [68]. The volume change of ferritic ductile iron has been measured by dilatometer on heating, and it was found that the contraction at the solid phase transformation decreased with higher amounts of copper. This was believed to be a result of the increased temperature range at which α- and γ-phases exist. The copper content was also found to influence the starting temperature of the ferrite to austenite transformation. This effect was compared to the lattice parameter, varying with copper contents [68].

Magnesium, in relation to cast iron, is perhaps best known as a means of modification of the graphite morphology. However, a magnesium addition has also some other effects; it has been shown that with increasing Mg contents the contraction of the material is greater [69]. Dilatation experiments with cast iron have shown that the level of magnesium influences the level of shrinkage. Increasing amounts of Mg increased the contraction. (Both expansion and contraction were found to be greater with increasing levels of magnesium [69].)

2.6. Calculations of Density—Modelling and Simulation

Several methods to calculate density can be found in the literature. An expression for calculations of density at an arbitrary temperature [4] is:

$$\rho_{T_x} = \rho_{T_0} + \Delta\rho = \ldots = \rho_{T_0} + \int_{T_0}^{T_1} \frac{\mathrm{d}\rho_1}{\mathrm{d}T_1}\mathrm{d}T + \int_{T_1}^{T_x} \frac{\mathrm{d}\rho_2}{\mathrm{d}T_2}\mathrm{d}T \tag{6}$$

where ρ_{T_0} is the density at eutectic temperature and $\Delta\rho$ is the change of density between arbitrary temperature T_x and eutectic temperature, T_0.

Several writers [3,7,70] have used the formula:

$$\rho = \rho_m + \Lambda\,(T - T_m) \tag{7}$$

where the temperature coefficient, Λ, at constant pressure is expressed as:

$$\Lambda = \left(\frac{\partial\rho}{\partial T}\right)_p \tag{8}$$

where ρ_m is the density at the melting point, T_m.

The generally known observation that there exists a relationship between the coefficient of thermal expansion at 20 °C and the melting temperature

$$\alpha_0 T_\mathrm{M} \cong 0.06 \tag{9}$$

for metals and semimetals [70] has been taken as a starting point for further work. Analogously, a similar relationship was shown to hold true for the liquid state.

For LGI, the expansion at eutectic temperature in the Fe-C-Si system has been found to co-vary with the modified carbon equivalent, CE* [9], which gave the linear function:

$$\frac{\Delta V}{V} = 1.57\,(\mathrm{CE}^* - 2.08) \tag{10}$$

where the modified carbon equivalent is written as:

$$\mathrm{CE}^* = (\%\,\mathrm{C}) + \frac{\%\mathrm{Si}}{5} \tag{11}$$

Moving towards the atomic scale, the following expression to calculate density [71] has been established:

$$\rho = \frac{\text{number of atoms of } X^* \text{ at wt of } X + \text{number of atoms of } Y^* \text{ at wt of } Y}{6.023 \times 10^{23} \times a \times b \times c} \tag{12}$$

where a, b, and c are lattice parameters.

2.6.1. Molar Volumes

Calculations of density can also be carried out by the use of molar volumes, V_m. The molar volume is the volume of one mole of a certain element at a certain pressure and temperature.

The fact that metal atoms are arranged in ordered crystal structures and that these may be of different appearances, e.g., cubic or hexagonal, gives rise to differences in solubility [72]. Moreover, the fcc structure has, for instance, greater interstitial spaces than the bcc structure, and elements like carbon and hydrogen can occupy this void [55].

Consequently, the alloying elements that make up cast iron will have to find a way to order themselves in a lattice structure. They do so either as interstitials or substitutionals. The total volume, V, of a system in which the alloying element is an interstitial, e.g., carbon in austenite, could be written as [73]:

$$V = \frac{n_{\mathrm{Fe}} N_{\mathrm{A}}}{4} (a_\gamma)^3, \tag{13}$$

The lattice parameter, a_γ, can be expressed as:

$$a_0 + m \frac{n_{\mathrm{c}} \times \text{at.wt. C} \times 100}{n_{\mathrm{Fe}} \times \text{at.wt. Fe} + n_{\mathrm{c}} \times \text{at.wt. C}}\,, \tag{14}$$

where n_{Fe} and n_{C} are number of moles of iron and carbon, N_{A} the Avogadro's number, and m is the slope of the lattice parameter versus the curve of wt. % C for a given temperature [74]. Lattice parameters are basically the edge lengths of the unit cell. In cubic crystals, the edge lengths are the same and usually denoted as a [75].

A statistical approach to the theory of conformal solutions, formulated in [76], could also be used [26]. The experimental results in this particular work were described by the equation:

$$V_m = \sum x_i \times {}^0V_i + \sum_i \sum_j x_i x_j \times I_{ij}, \tag{15}$$

where ${}^0V_i$ is the volume of the pure components i, x_i is themolar fraction of atom i, and I_{ij} is the parameters representing deviation from ideal behavior. (This general form is found in [77], which is built on the same theoretical background.)

The most well-known interstitial in cast iron would be carbon, placed in the voids of the iron fcc-lattice. One way to model this is by the use of a sub-lattice model. Iron and other large atoms are then placed in one lattice and the interstitials in a second one. Should there be no interstitials, the second lattice will display only vacancies. The density calculated from the molar volume is then computed as analogous to the general density equation, i.e.,:

$$\rho = \frac{M}{V_m}, \tag{16}$$

where M is the molar weight. In a multiphase alloy, the density can be calculated as:

$$\rho = \sum f_v \times \rho_i \,, \tag{17}$$

where f_v is the volume fraction of the phase and ρ_i is the density of the same phase [77].

Austenite can be considered a solid solution of iron and silicon in a substitutional matrix with carbon as interstitial [65].

From the definition of the coefficient of thermal expansion (α) [78] the following expression could be derived:

$$V_m(T) = V_0 \, \exp(\int_{T_0}^{T} 3\alpha \mathrm{d}T) + \Delta V_m^{\mathrm{magn}}(T) \,, \tag{18}$$

where V_0 is the molar volume at the reference temperature, T_0 is the reference temperature, $\Delta V_m^{\mathrm{magn}}$ is the the magnetic contribution to the molar volume, and 3α is the coefficient of thermal expansion (α) of a phase in the nonmagnetic state in a cubic element [78].

Another way of expressing the molar volume is by taking the excess volume into consideration [7]. The molar volume for a liquid solution with the components A_i (i ranging from 1 to n) can then be described as:

$$V = \sum_{i=1}^{n} c_i \frac{M_i}{\rho_i} + V^{\mathrm{E}}, \tag{19}$$

where c_i is the atomic concentration, M_i is the molar mass, ρ_i is the density of the pure substance at T, and V^{E} is the excess volume.

2.6.2. Balance Equations with Control Volume

Density can be related to thermodynamic variables and expressed by a truncated Taylor series [79]. The calculations can be done using a control volume; this volume element can be chosen to include both liquid and solid phases, as are the conditions in the mushy zone. Figure 5 shows an example of a control volume that could be taken at the surface of a dendrite.

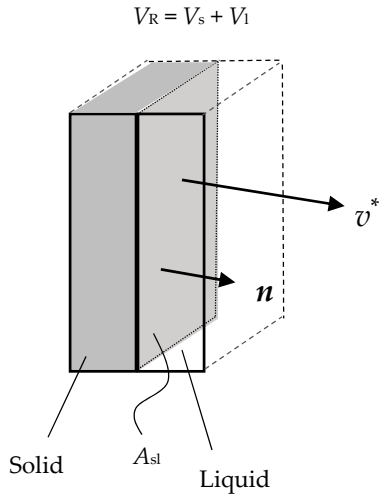

Figure 5. Control volume. A_{sl} is the interface area, $\boldsymbol{n}$ is the vector normal to A_{sl}, and v^* is the moving velocity. V_R is the volume of the control volume, combined with the solid, V_s, and liquid, V_l, components. Redrawn from Dantzig and Rappaz [79] (p. 112).

Control volumes can also contain just one single phase, i.e., either solid or liquid. By the use of such a single-phase control volume, the mass balance in, for example, the x-direction can be constructed

to eventually give Equation (20). The mass flux through the surface of the control volume will give the rate of mass change inside the volume:

$$\int_V \frac{\partial \rho}{\partial t} \mathrm{d}V + \int_A \rho \boldsymbol{v} \cdot \boldsymbol{n} \, dA = 0 \,, \tag{20}$$

where ρ is the density, t is the time, V is the volume, A is the area, $\boldsymbol{v}$ is the velocity (vector), and $\boldsymbol{n}$ is the normal (vector).

Applying the above equation (Equation (20)) to a control volume (Figure 6) at the solid-liquid interface, and considering the solid as fixed (i.e., $\boldsymbol{v}_s^* = 0$), the following expression can be obtained:

$$\boldsymbol{v}_l^* \cdot \boldsymbol{n} = \frac{\rho_l - \rho_s}{\rho_l} \boldsymbol{v}^* \cdot \boldsymbol{n} = -\beta \boldsymbol{v}^* \cdot \boldsymbol{n}, \tag{21}$$

(Subscripts l and s are for liquid and solid. The star indicates evaluation at the liquid-solid interface.) The solidification shrinkage factor, β, can be represented as:

$$\beta = \frac{\rho_l - \rho_s}{\rho_l}, \tag{22}$$

For most materials, the solidification shrinkage factor can be represented as $\beta > 0$. A notable exception is however Si [79].

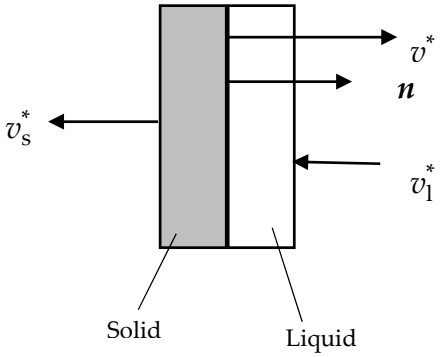

Figure 6. Control volume at the solid-liquid interface. Redrawn (and simplified) from Dantzig and Rappaz [79] (p. 117).

2.6.3. Expressions Based on Morphology

Expressions describing the morphology of the dendritic and inter-dendritic spaces are important also when it comes to density measurements. The modulus of primary dendrite was developed to describe the coarseness of the primary phase (as an alternative to the SDAS). The hydraulic diameter is describing the interspace between the dendrites [80]. The modulus of the primary dendrite is:

$$M_{\mathrm{PD}} = \frac{V_\gamma}{S_\gamma} \,, \tag{23}$$

where V_γ is volume primary austenite and S_γ is the surface area (envelope) of the austenite dendrite. The hydraulic diameter is:

$$D_{\mathrm{IP}}^{\mathrm{Hyd}} = \frac{V_{\mathrm{IP}}}{S_\gamma} \,, \tag{24}$$

where V_{IP} is the volume of the inter-dendritic space. It has been found that, in areas where the local solidification time is long, the inter-dendritic space is large [81]. These areas could also be connected to shrinkage porosities or metal expansion penetration.

From solidification modelling of thermo-physical properties, it has been found that deviations from what can be called an ideal mixing involve a volume contraction. The magnitude of this contraction is said to be strongly governed by the magnitude of the thermodynamic interaction [82].

Faster growing phases show a greater number of lattice defects. It has been shown (on SGI) that, if the number of defects in the austenite lattice is high, the activity of carbon decreases. This means that the solubility of carbon in lattice affects austenite increases. Vacancy may exist in the lattice structure, and pore formation can be described as the condensing of vacancies. It has also been suggested that the entropy for formation of vacancies is concentration dependent [83].

Volume changes during the solidification of LGI have been concluded [11] to be influenced by factors such as the precipitation of primary austenite and carbon content in the area of the eutectic solidification. Further, the solidification time locally, the undercooling, and the number of eutectic cells are all factors that will have an influence. Moreover, it has also been reported that cylindrical samples display an anisotropic behaviour when volume change has been measured in axial and radial directions [84].

3. Conclusions

Reviewing the different measurement methods, it is clear that they all have their advantages and disadvantages. Aspects influencing the measurements must be taken into consideration and corrections must often be made. Since there is not just one ideal method, it must be clear to the scientist which parameters are important and at which point yielding is necessary when selecting an appropriate experimental setup.

One important issue to consider, if the sample is remelted in the experiment, is that the material will not be exactly the same as in the initial sample after solidification. It is also important to be aware of the fact that the surrounding environment affects the sample, i.e., reactions between the measurement equipment (container, sinker etc.) and the sample will affect the result.

Most methods measure density during a shorter temperature interval, though with the exception of dilatometry, by which it is possible to continuously monitor the expansion and contraction behaviour during a larger temperature interval, e.g., from superheated melt to room temperature.

Taking the aspects of the ability to monitor the volume changes of a material during solidification and the issues of remelting already cast material, the liquid to solid dilatometer would be the most appropriate measurement method for cast iron.

In predicting casting outcomes, the industry relies heavily on simulation. In order to minimize the occurrence of defects like shrinkage porosity (which will lead to the scrapping of cast and often machined components), apt tools are of essence. To create these tools, a thorough knowledge of the density changes the material goes through during solidification and how to model these changes is needed. Since density measurement data for molten cast irons are difficult to find and because the range of chemical composition and graphite morphology for those data is limited, there is a need for further investigations to cover the area. These investigations should also be compared with data obtained through different calculation methods.

More research on how alloying elements affect the density of the different varieties of cast iron is also needed. Solubility and mixing laws and their application for cast iron should be further investigated.

Acknowledgments: The present work was realised partly within the SPOFIC (Shrinkage Porosity Formation in Compacted Graphite Iron) I & II project funded from the Swedish Vinnova agency and partly within the project Appointment of Professorship in Foundry Technology at Jönköping University, financed by the Swedish Knowledge Foundation, Scania CV AB, Volvo Group Trucks Operations and Jönköping University. All participating partners are greatly acknowledged.

Author Contributions: Attila Diószegi provided the idea for the paper, Kristina Hellström researched and wrote the paper, Lucian Diaconu contributed with diagrams. Attila Diószegi and Lucian Diaconu reviewed the paper.

Conflicts of Interest: The authors declare no conflict of interest.

References

1. Saito, T.; Shiraish, Y.; Sakuma, Y. Density measurement of molten metals by levitation technique at temperatures between 1800 degrees C and 2200 degrees C. *Trans. Iron Steel Inst. Jpn.* **1969**, *9*, 118–126.
2. Mills, K.C. *Recomended Values of Thermophysical Properties for Selected Commercial Alloys*; Woodhead Publishing: Cambridge, UK, 2002.
3. Jimbo, I.; Cramb, A.W. The density of liquid iron-carbon alloys. *Metall. Trans. B* **1993**, *24*, 5–10. [CrossRef]
4. Kusakawa, T.; Kim, S.; Kondo, T. *Volume Change of Molten Spheroidal Graphite Cast Iron*; Report of the Castings Research Laboratory; Waseda University: Tokyo, Japan, 1972; pp. 23–32.
5. Blumm, J.; Henderson, J.B. Measurement of the volumetric expansion bulk density of metals in the solid and molten regions. *High Temp. High Press.* **2000**, *32*, 109–113. [CrossRef]
6. Mizukami, H.; Yamanaka, A.; Watanabe, T. Prediction of density of carbon steels. *ISIJ Int.* **2002**, *42*, 375–384. [CrossRef]
7. Brillo, J.; Egry, I. Density of multicomponent melts measured by electromagnetic levitation. *Jpn. J. Appl. Phys.* **2011**, *50*, 11RD02. [CrossRef]
8. Mills, K.C. Measurement and estimation of physical properties of metals at high temperatures. In *Fundamentals of Metallurgy*; Seetharaman, S., Ed.; Woodhead Publishing Ltd: Cambridge, UK, 2005; pp. 109–177.
9. Kagawa, A.; Kiguchi, S.; Osada, M. Volumetric change in freezing cast irons. *Trans. Jpn. Foundrym. Soc.* **1995**, *18*, 18–23.
10. Stefanescu, D.M.; Moran, M.; Boonmee, S.; Guesser, W.L. The use of combined liquid displacement and cooling curve analysis in understanding the solidification of cast iron. *AFS Trans.* **2012**, *120*, 365–374.
11. Tadesse, A.; Fredriksson, H. Volume change during the solidification of grey cast iron: Its relation with the microstructural variation, comparison between experimental and theoretical analysis. *Int. J. Cast Met. Res.* **2017**, *30*, 159–170. [CrossRef]
12. Bäckerud, L.; Nilsson, K.; Steen, H. Study of nucleation and growth of graphite in magnesium-treated cast iron by means of thermal analysis. In Proceedings of the 2nd International Symposium on the Metallurgy of Cast Iron, Geneva, Switzerland, 29–31 May 1974; pp. 625–637.
13. Svensson, I.L. *Component Casting with Simulation*; School of Engineering Jönköping University: Jönköping, Sweden, 2002.
14. König, M.; Wessén, M. Influence of alloying elements on microstructure and mechanical properties of CGI. *Int. J. Cast Met. Res.* **2010**, *23*, 97–110. [CrossRef]
15. Stefanescu, D. Solidification and modelling of cast iron—A short history of the defining moments. *Mater. Sci. Eng. A* **2005**, *413*, 322–333. [CrossRef]
16. Narendranath, C.S.; Srinivasan, M.N. Effect of cooling rate variables on the solidification times and microstructure of permanent mold magnesium-treated iron castings. *J. Test. Eval.* **1995**, *23*, 281–287.
17. Stefanescu, D.M. *Science and Engineering of Casting Solidification*, 2nd ed.; Springer: New York, NY, USA, 2009.
18. Rivera, G.; Boeri, R.; Sikora, J. Solidification of gray cast iron. *Scr. Mater.* **2004**, *50*, 331–335. [CrossRef]
19. Rivera, G.L.; Boeri, R.E.; Sikora, J.A. Searching for a unified explanation of the solidification of cast irons. In Proceedings of the Eighth International Symposium on Science and Processing of Cast Iron, Beijing, China, 16–19 October 2006; Tsinghua University Press: Beijing, China, 2006.; pp. 45–50.
20. Young, H.D.; Freedman, R.A. *University Physics*, 10th ed.; Addison Wesley Longman: San Francisco, CA, USA, 2000.
21. Kirshenbaum, A.D.; Cahill, J.A. The density of liquid iron from the melting point to 2500 K. *Trans. Metall. Soc. AIME* **1962**, *224*, 816–819.
22. Lucas, L.-D. Densité de métaux à haute température (dans les états solide et liquide). *Deux. Partie. Mém. Sci. Rev. Métall.* **1972**, *60*, 479–492.
23. Lucas, L.D. Techniques of metals research. In *Physiochemical Measurements in Metals Research*; Rapp, R.A., Ed.; John Wiley & Sons: New York, NY, USA, 1970; Volume IV, Part 2.
24. Lucas, L.-D. Volume spécifique de métaux et alliages liquides à hautes températures. *Prem. Partie. Mem. Scie. Rev. Metall.* **1964**, *61*, 1–24.

25. Assael, M.J.; Kakosimos, K.; Banish, R.M.; Brillo, J.; Egry, I.; Brooks, R.; Quested, P.N.; Mills, K.C.; Nagashima, A.; Sato, Y.; et al. Reference data for the density and viscosity of liquid aluminum and liquid iron. *J. Phys. Chem. Ref. Data* **2006**, *35*, 285–300. [CrossRef]
26. Olsson, A. The influence of C, Si and Mo on the density of liquid iron. *Scand. J. Metall.* **1981**, *10*, 263–271.
27. Dubberstein, T.; Heller, H.P.; Klostermann, J.; Schwarze, R.; Brillo, J. Surface tension and density data for Fe-Cr-Mo, Fe-Cr-Ni, and Fe-Cr-Mn-Ni steels. *J. Mater. Sci.* **2015**, *50*, 7227–7237. [CrossRef]
28. Langen, M.; Hibiya, T.; Eguchi, M.; Egry, I. Measurement of the density and the thermal expansion coefficient of molten silicon using electromagnetic levitation. *J. Cryst. Growth* **1998**, *186*, 550–556. [CrossRef]
29. Wille, G.; Millot, F.; Rifflet, J.C. Thermophysical properties of containerless liquid iron up to 2500 K. *Int. J. Thermophys.* **2002**, *23*, 1197–1206. [CrossRef]
30. Gorges, E.; Raez, L.M.; Schillings, A.; Egry, I. Density measurements on levitated liquid metal droplets. *Int. J. Thermophys.* **1996**, *17*, 1163–1172. [CrossRef]
31. Yoo, H.; Park, C.; Jeon, S.; Lee, S.; Lee, G.W. Uncertainty evaluation for density measurements of molten Ni, Zr, Nb and Hf by using a containerless method. *Metrologia* **2015**, *52*, 677–684. [CrossRef]
32. Brillo, J.; Egry, I. Density and excess volume of liquid copper, nickel, iron, and their binary alloys. *Z. Fur Metallkunde* **2004**, *95*, 691–697. [CrossRef]
33. Smith, P.M.; Elmer, J.W.; Gallegos, G.F. Measurement of the density of liquid aluminum alloys by an X-ray attenuation technique. *Scr. Mater.* **1999**, *40*, 937–941. [CrossRef]
34. Terasaki, H.; Nishida, K.; Shibazaki, Y.; Sakamaki, T.; Suzuki, A.; Ohtani, E.; Kikegawa, T. Density measurement of Fe_3C liquid using X-ray absorption image up to 10 GPa and effect of light elements on compressibility of liquid iron. *J. Geophys. Res. Solid Earth* **2010**, *115*. [CrossRef]
35. Sanloup, C.; Guyot, F.; Gillet, P.; Fiquet, G.; Mezouar, M.; Martinez, I. Density measurements of liquid Fe-S alloys at high-pressure. *Geophys. Res. Lett.* **2000**, *27*, 811–814. [CrossRef]
36. Mehmood, S.; Klotz, U.E.; Pottlacher, G. Thermophysical properties of platinum-copper alloys. *Metall. Mater. Trans.* **2012**, *43*, 5029–5037. [CrossRef]
37. Huepf, T.; Cagran, C.; Kaschnitz, E.; Pottlacher, G. Thermophysical properties of Ni80Cr20. *Thermochim. Acta* **2009**, *494*, 40–44. [CrossRef]
38. Wilthan, B.; Cagran, C.; Brunner, C.; Pottlacher, G. Thermophysical properties of solid and liquid platinum. *Thermochim. Acta* **2004**, *415*, 47–54. [CrossRef]
39. Yamada, N.; Abe, R.; Okaji, M. A calibration method for measuring thermal expansions with a push-rod dilatometer. *Meas. Sci. Technol. (UK)* **2001**, *12*, 2121–2129. [CrossRef]
40. Mohapatra, G.; Sommer, F.; Mittemeijer, E.J. The austenite to ferrite transformation of Fe-Ni under the influence of a uniaxially applied tensile stress. *Acta Mater.* **2007**, *55*, 4359–4368. [CrossRef]
41. Frankel, J.I.; Porter, W.D.; Sabau, A. Analysis of volumetric changes through melting using a dilatometer. *J. Therm. Anal. Calorim.* **2005**, *82*, 171–177. [CrossRef]
42. Westcot, E.J.; Binet, C.; German, R.M. In situ dimensional change, mass loss and mechanisms for solvent debinding of powder injection moulded components. *Powder Metall.* **2003**, *46*, 61–67. [CrossRef]
43. Reed, R.C.; Akbay, T.; Shen, Z.; Robinson, J.M.; Root, J.H. Determination of reaustenitisation kinetics in a Fe-0.4C steel using dilatometry and neutron diffraction. *Mater. Sci. Eng. A (Switzerland)* **1998**, *256*, 152–165. [CrossRef]
44. Sandeep Kumar, T.K.; Viswanathan, N.N.; Ahmed, H.M.; Andersson, C.; Björkman, B. Estimation of sintering kinetics of oxidized magnetite pellet using optical dilatometer. *Metall. Mater. Trans.* **2015**, *46*, 635–643. [CrossRef]
45. Piasecki, M.; Lakshminarayana, G.; Fedorchuk, A.O.; Kushnir, O.S.; Franiv, V.A.; Franiv, A.V.; Myronchuk, G.; Plucinski, K.J. Temperature operated infrared nonlinear optical materials based on Tl4HgI6. *J. Mater. Sci. Mater. Electron.* **2013**, *24*, 1187–1193. [CrossRef]
46. Roach, S.J.; Henein, H. Physical properties of AZ91D measured using the draining crucible method: Effect of SF_6. *Int. J. Thermophys.* **2012**, *33*, 484–494. [CrossRef]
47. Roach, S.J.; Henein, H. A new method to dynamically measure the surface tension, viscosity, and density of melts. *Metall. Mater. Trans. B* **2005**, *36*, 667–676. [CrossRef]
48. Morard, G.; Garbarino, G.; Antonangeli, D.; Andrault, D.; Guignot, N.; Siebert, J.; Roberge, M.; Boulard, E.; Lincot, A.; Denoeud, A.; et al. Density measurements and structural properties of liquid and amorphous metals under high pressure. *High Press. Res.* **2014**, *34*, 9–21. [CrossRef]

49. Cottrell, A.H. *Theoretical Structural Metallurgy*; Edward Arnold & Co.: London, UK, 1953.
50. Davis, J.R. Metals handbook. In *Basic Metallurgy of Cast Iron*, 2nd ed.; Davis, J.R., Ed.; ASM International Handbook Committee: Geauga County, OH, USA, 1998; pp. 307–309.
51. Goodrich, G.M. Composition of cast irons. In *ASM Handbook*; ASM International: Geauga County, OH, USA, 2008; Volume 15, pp. 785–811.
52. Stefanescu, D.M. Principles of the metallurgy of cast iron. In *ASM Handbook*; ASM International: Geauga County, OH, USA, 1990; Volume 1, pp. 3–11.
53. Jönköping University. *Course on Metallurgy, Solidification and Modelling of Cast Iron Castings*, 4th ed. Available online: http://ju.se/download/18.1b4209714cfb031d01cf0/1439277281982/Cast_iron_course_150518.pdf (accessed on 13 April 2017).
54. Elmquist, L.; Soivio, K.; Diószegi, A. Cast iron solidification structure and how it is related to defect formation. *Mater. Sci. Forum* **2014**, *790*, 441–446. [CrossRef]
55. Brennert, S. *Materiallära*; Liber Utbildning: Solna, Sweden, 1993.
56. Minkoff, I. Crystal growth theory and cast iron structures. *Phys. Metall. Cast Iron IV* **1989**, 3–13.
57. Slack, G.A.; Bartram, S.F. Thermal expansion of some diamondlike crystals. *J. Appl. Phys.* **1975**, *46*, 89–98. [CrossRef]
58. Ekbom, L. Grundämnestabell. In *Mafyke. Tabeller och Formler N T Te*; Almqvist & Wiksell: Stockholm, Sweden, 1991; pp. 95–97.
59. Ledbetter, H.M.; Austin, M.W. Dilation of an fcc Fe-Cr-Ni alloy by interstitial carbon and nitrogen. *Mater. Sci. Technol.* **1987**, *3*, 101–104. [CrossRef]
60. Stuart, H.; Ridley, N. Thermal expansion of cementite and other phases. *J. Iron Steel Inst.* **1966**, *204*, 711–717.
61. *A Periodic Table of the Elements. Printed Poster*; The Royal Society of Chemistry: London, UK, 1987.
62. Silicon (Si). Available online: http://academic.eb.com/EBchecked/topic/544301/silicon (accessed on 10 December 2015).
63. Zulehner, W.; Neuer, B.; Rau, G. Silicon. In *Ullmann's Encyclopedia of Industrial Chemistry*; Wiley-VCH Verlag: Weinheim, Germany, 2000.
64. Vazehrad, S.; Elfsberg, J.; Diószegi, A. Study of microstructure and silicon segregation in cast iron using color etching and electron microprobe analysis. *Mater. Charact.* **2014**, *104*, 132–138. [CrossRef]
65. Chen, Q.; Langer, E.W.; Hansen, P.N. Relationship between specific volume, chemical composition, and fraction of austenite, graphite and cementite during eutectic reaction of cast iron. *Scand. J. Metall.* **1994**, *23*, 3–8.
66. Mazur, A.V.; Gasik, M.M. Thermal expansion of silicon at temperatures up to 1100 degree C. *J. Mater. Process. Technol.* **2009**, *209*, 723–727. [CrossRef]
67. Ledbetter, H.M.; Austin, M.W. Molybdenum effect on volume in Fe-Cr-Ni alloys. *J. Mater. Sci.* **1988**, *23*, 3120–3124. [CrossRef]
68. Choe, K.-H.; Lee, S.-M.; Kim, M.-H.; Lee, K.-W. The effect of Cu on the microstructure and the elevated temperature properties of ferritic heat resistant cast iron. *Mater. Sci. Forum* **2010**, *654*, 1448–1451. [CrossRef]
69. Hummer, R. Relationship between cooling and dilatation curves of ductile-iron melts and their shrinkage tendency. *Cast Met.* **1988**, *1*, 62–68. [CrossRef]
70. Steinberg, D.J. A simple relationship between the temperature dependence of the density of liquid metals and their boiling temperatures. *Metall. Trans.* **1974**, *5*, 1341–1343. [CrossRef]
71. Heine, R.W. A model for specific volume and expansion and contration behavior of solidifying and cooling ductile and gray iron. *AFS Trans.* **1988**, *96*, 413–422.
72. Bailey, A.R. *A Text-Book of Metallurgy*; Macmillan and Co.: London, UK, 1954.
73. Trivedi, R.; Pound, G.M. Calculations of partial molal volumes in Fe-C system. *Acta Metall.* **1967**, *15*, 1761–1762. [CrossRef]
74. Ridley, N.; Stuart, H. Partial molar volumes from high-temperature lattice parameters of iron-carbon austenites. *Met. Sci. J.* **1970**, *4*, 219–222. [CrossRef]
75. Gottstein, G. *Physical Foundations of Materials Science*; Springer: Berlin/Heidelberg, Germany, 2004.
76. Longuet-Higgins, H.C. The statistical thermodynamics of multicomponent systems. In *Proceedings of the Royal Society of London Series A: Mathematical and Physical Sciences*; The Royal Society: London, UK, 1951; Volume 205, pp. 247–269.

77. Svensson, I.L.; Diószegi, A. On modelling of volume related defect formation in cast irons. In Proceedings of the 9th International Conference on Modelling of Casting, Welding and Advanced Solidification Processes IX, Aachen, Germany, 20–25 August 2000.
78. Lu, X.-G.; Selleby, M.; Sundman, B. Theoretical modeling of molar volume and thermal expansion. *Acta Mater.* **2005**, *53*, 2259–2272. [CrossRef]
79. Dantzig, J.A.; Rappaz, M. *Solidification*, 1st ed.; CRC Press: Boca Raton, FL, USA, 2009.
80. Lora, R.; Diószegi, A.; Fourlakidis, V.; Vilaseca, G.P.; Osona, A.D. *Characterization of the Primary Austenite Dendrite and Interdendritic Space in Lamellar Cast Iron*; Jönköping University: Jönköping, Sweden, 2011.
81. Svidró, P. Study of Solidification and Volume Change in Lamellar Cast Iron with Respect to Defect Formation Mechanisms. Master's Thesis, Royal Insitute of Technology (KTH), Stockholm, Sweden, 2013.
82. Saunders, N.; Li, X.; Miodownik, A.P.; Schillé, J.-P. Modelling of the thermo-physical and physical properties relevant to solidification. *Adv. Solidif. Process. X* **2003**.
83. Fredriksson, H.; Stjerndahl, J.; Tinoco, J. On the solidification of nodular cast iron and its relation to the expansion and contraction. *Mater. Sci. Eng. A* **2005**, *413*, 363–372. [CrossRef]
84. Svidró, P.; Diószegi, A. On the problems of volume change measurements in lamellar cast iron. *Int. J. Cast Met. Res.* **2014**, *27*, 26–37. [CrossRef]